
TXT-tool 3.081-1.2 Simulation of Landslide Induced Tsunami (LS-Tsunami) Based on the Landslide Motion Predicted by LS-RAPID

Khang Dang, Kyoji Sassa, Hideaki Yanagisawa
and Bin He

Abstract

By combining landslide dynamics research and tsunami research, we present an integrated series of numerical models quantitatively simulating the complete evolution of a landslide-induced tsunami. The integrated model simulating the landslide initiation and motion uses measured landslide dynamic parameters from a high-stress undrained dynamic-loading ring shear apparatus. It provides the numerical data of a landslide mass entering and moving under water to the tsunami simulation model as the trigger of tsunami. The series of landslide and tsunami simulation models were applied to the 1792 Unzen-Mayuyama megaslide and the ensuing tsunami disaster, which is the largest landslide disaster, the largest volcanic disaster and the largest landslide-induced tsunami disaster to have occurred in Japan. Both the 1792 megaslide and the tsunami portions of the disaster are well documented, making this an excellent test of the reliability and precision of the new simulation model. The simulated tsunami heights at the coasts well match the historical tsunami heights recorded by “Tsunami-Dome-Ishi” (a stone showing the tsunami reaching point) and memorial stone pillars.

Keywords

Unzen-Mayuyama landslide · Landslide-induced tsunami
Undrained ring shear test · Computer simulation

K. Dang · K. Sassa (✉)
International Consortium on Landslides, 138-1,
Tanaka Asukaicho, Sakyo-Ku, Kyoto 606-8226,
Japan
e-mail: sassa@iclhq.org

K. Dang
VNU University of Science, Hanoi, Vietnam

H. Yanagisawa
Department of Regional Design, Faculty of Liberal
Arts, Tohoku Gakuin University, Sendai, Japan

B. He
State Key Laboratory of Lake Science and
Environment, Nanjing Institute of Geography and
Limnology, Chinese Academy of Science, Nanjing,
China
e-mail: hebin@niglas.ac.cn

Contents

1	Introduction	112
2	Basic Principle of the Landslide-Induced Tsunami Model	112
3	Two Sets of Equations to Simulate Landslide Motion and Tsunami Motion	114
4	Application of the Model to Two Hypothetical Simple Coastal Landslides	116
5	Application of the Model to the Unzen-Mayuyama Landslide and Its Resulting Tsunami Wave	119
6	Conclusion	128
	References.....	129

1 Introduction

A new 3-D landslide dynamics model (LS-RAPID) has been developed integrating the initiation and motion of landslides based on measured landslide dynamic parameters (Sassa et al. 2010). We have decided to use the landslide motion simulated by LS-RAPID as the trigger of tsunami. The tsunami simulation model used in this study is a well established and widely used model (IOC, 1997). We assumed that horizontal forces between landslide mass and water can be neglected, and tsunami is triggered only by upheaved water mass on the submarine ground due to a moving landslide mass. This assumption is the same with Baba et al. (2012), Abe et al. (2008) and Satake (2001). The tsunami simulation code using the landslide motion data from LS-RAPID was developed (LS-Tsunami) for this study.

The objective of this paper is to define the precision of the series of landslide-induced tsunami models (LS-RAPID + LS-Tsunami). The 1792 Unzen-Mayuyama landslide-and-tsunami disaster was selected as the test case to examine the precision. Both the initial landslide, the landslide displacement, and the tsunami disaster were well investigated and documented. This

landslide (volume $3.4 \times 10^8 \text{ m}^3$; maximum depth 400 m) killed 10,139 persons directly by the displaced landslide mass and also by the triggered tsunami wave in the Shimabara Peninsula. The landslide-induced tsunami crossed the Ariake Sea and killed 4653 people in Kumamoto Prefecture on the opposite bank, 343 people on Amakusa Island and 18 people in other areas (Usami 1996). Sassa et al. investigated the Unzen Mayuyama landslide by measuring the appropriate dynamic parameters for two samples taken from the site using a newly developed high-stress undrained ring-shear apparatus (up to 3 MPa in normal stress and pore pressure). The LS-RAPID simulation using these parameters successfully reproduced the motion of the 1792 Unzen-Mayuyama megaslide in Japan (Sassa et al. 2014a, b). Those measured landslide dynamics parameter are used in this study.

2 Basic Principle of the Landslide-Induced Tsunami Model

The basic principle of the landslide-induced tsunami model used in this study is illustrated in Fig. 1. The left part of Fig. 1 is same as the principle of the integrated landslide simulation model (LS-RAPID) of Sassa et al. (2010). The only difference here is that the landslide mass is located beneath a water surface. The right part of Fig. 1 illustrates the elevated water mass (which causes a tsunami wave) by the upward displacement of the interface between the landslide and the water due to the movement of the landslide mass over the sea floor.

When the landslide mass enters or travels across the sea floor, the elevation of the submarine ground surface (which is the interface of landslide mass and submarine water) will be increased. The submarine ground surface elevated by the landslide mass will raise the water

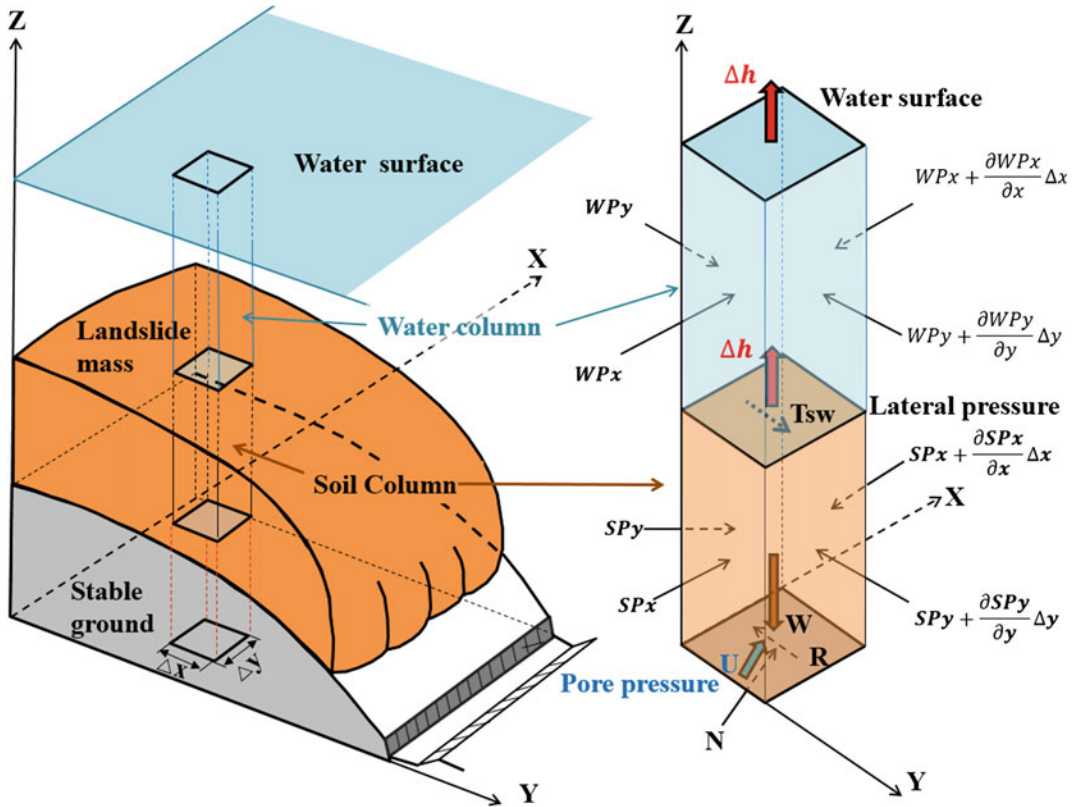


Fig. 1 Basic principle of the landslide-induced tsunami simulation model

mass above the landslide-water interface by an amount, Δh , in a unit time, Δt . The shear resistance (τ_{sw}) between soil and water at this interface should be much smaller than the shear resistance within the soil. Hence, this resistance, τ_{sw} was ignored in the simulation. The effective stress acting on the surface between the bottom of the soil column and the top of the sea floor was regarded as being unaffected by the increase in water height for the following two reasons: (1) the surficial deposit on the sea floor is unconsolidated, and hence is expected to be permeable enough to transmit the water-pressure change due to water height change to the bottom of the soil column above the sea floor; and (2) the soil column of the moving mass is both unconsolidated and water saturated, hence the transmission of water-pressure change from the top of soil column to the bottom of the soil column is fast (elastic wave velocity of water is around 1.5 km/s) and can be regarded as instantaneous.

When a landslide mass enters into water, the buoyant force by water will act on the soil mass. Namely the unit weight of soil mass (γ_t) on land will change to the buoyant unit weight of soil mass, the difference between γ_t and γ_w (unit weight of sea water) under water. In the case of partial submersion, the buoyant force by water will act only on the part of soil mass below the water surface. No tangential force between soil and water is considered because the tangential force by water will be negligible compared to the shear resistance mobilized in the shear surface of large-scale landslides.

There are many parameters to regulate landslide motion on land (Sassa et al. 2010, 2014a, b) and submarine landslide motion (Sassa et al. 2012). The values of such landslide dynamics parameters were mostly measured by the undrained ring shear testing on the samples taken from the landslide source area and its moving area. The parameters used in tsunami simulation

(LS-Tsunami) are the unit weight of sea water and Manning's roughness coefficient for basal resistance between water and ground.

3 Two Sets of Equations to Simulate Landslide Motion and Tsunami Motion

The calculation part of the landslide-induced tsunami model contains the following two steps.

The first step: simulation of landslide mass by the integrated landslide simulation model "LS-RAPID" on land and on the sea floor. The equations of the first step are (1)–(4), which are the same as in LS-RAPID (Sassa et al. 2010).

The second step: simulation of the tsunami by LS-Tsunami. The equations of the second step are (5)–(8), which is an established tsunami simulation model (IOC 1997).

The concept of LS-RAPID is that the acceleration (a) of the soil mass (m_s) is induced by the sum of forces of the self-weight of soil mass, the seismic force acting on the soil column, the shear force acting on the bottom of soil column, and lateral pressure acting on the sides of the soil column (Eq. 1).

The concept of the landslide-induced tsunami simulation (LS-Tsunami) is that the acceleration (a) of the water mass (m_w) is induced by the sum of forces of the lateral pressure acting on the sides of the water column and the Manning's basal shear resistance due to roughness of the ground (Eq. 5). Both sets of equations are shown from (1) to (8) below.

Basic Equations for Motion of Landslide (LS-RAPID)

$$am_s = (W + F_v + F_x + F_y) + \left(\frac{\partial P_x}{\partial x} \Delta x + \frac{\partial P_y}{\partial y} \Delta y \right) R \quad (1)$$

where

a Acceleration of a soil column,
 m_s : landslide mass in a column;
 W Self-weight of column,

F_v, F_x, F_y Three components of seismic forces;

$\frac{\partial P_x}{\partial x} \Delta x, \frac{\partial P_y}{\partial y} \Delta y$ Lateral pressure acting on the side walls of the column in the x and y directions;

R Shear resistance acting on the base of the column.

Expressing Eq. (1) in x, y directions, Eqs. (2) and (3) are obtained. Assuming the total mass of landslide does not change during motion, Eq. (4) is obtained.

$$\begin{aligned} & \frac{\partial M}{\partial t} + \frac{\partial}{\partial x}(u_0 M) + \frac{\partial}{\partial y}(v_0 M) \\ &= gh \left\{ \frac{\tan \alpha}{q+1} (1 + Kv) + Kx \cos^2 \alpha \right\} - (1 + Kv) kgh \frac{\partial h}{\partial x} \\ & \quad - \frac{g}{(q+1)^{1/2}} \cdot \frac{u_0}{(u_0^2 + v_0^2 + w_0^2)^{1/2}} \{ h_c (q+1) \\ & \quad + (1 - r_u) h \tan \phi_a \} \end{aligned} \quad (2)$$

$$\begin{aligned} & \frac{\partial N}{\partial t} + \frac{\partial}{\partial x}(u_0 N) + \frac{\partial}{\partial y}(v_0 N) \\ &= gh \left\{ \frac{\tan \beta}{q+1} (1 + Kv) + Ky \cos^2 \beta \right\} \\ & \quad - (1 + Kv) kgh \frac{\partial h}{\partial y} - \frac{g}{(q+1)^{1/2}} \cdot \\ & \quad \frac{v_0}{(u_0^2 + v_0^2 + w_0^2)^{1/2}} \{ h_c (q+1) + (1 - r_u) h \tan \phi_a \} \end{aligned} \quad (3)$$

$$\frac{\partial h}{\partial t} + \frac{\partial M}{\partial x} + \frac{\partial N}{\partial y} = 0 \quad (4)$$

where

h Height of soil column within a mesh;
 u_0, v_0 Velocity of a soil column to X and Y directions, respectively (velocity distribution in Z direction is neglected, and assumed to be a constant);

M, N Discharge of soil per unit width in X and Y directions respectively ($M = u_0 h, N = v_0 h$);

g Acceleration due to gravity;

α, β

	Angles of the ground surface to X–Z plain and Y–Z plain, respectively;
k	Lateral pressure ratio (ratio of lateral pressure and vertical pressure);
$\tan \phi_a$	Apparent friction coefficient mobilized at the sliding surface of landslide;
hc	Cohesion c expressed in the unit of height ($c = \rho g hc$, ρ : density of soil);
r_u	Pore pressure ratio (u/σ);
K_v, K_x, K_y	Seismic coefficients to the vertical, x and y directions;

$$q = \tan^2 \alpha + \tan^2 \beta$$

$$w_0 = -(u_0 \tan \alpha + v_0 \tan \beta)$$

Basic Equations for Motion of Water (LS-Tsunami)

$$am_w = \frac{\partial P_x}{\partial x} \Delta x + \frac{\partial P_y}{\partial y} \Delta y + R(\text{Manning}) \quad (5)$$

where

a	Acceleration of a water column;
m_w	Water mass in a column;
R(Manning)	Manning's basal resistance between water and ground;
$\frac{\partial P_x}{\partial x} \Delta x, \frac{\partial P_y}{\partial y} \Delta y$	Lateral pressure acting on the side wall of column in x and y directions.

Equation (5) is expressed by Eqs. (6), (7) and (8).

$$\frac{\partial M}{\partial t} + \frac{\partial}{\partial x}(u_0 M) + \frac{\partial}{\partial y}(v_0 M) = -gh \frac{\partial \eta}{\partial x} - \frac{\tau_x}{\rho} \quad (6)$$

$$\frac{\partial N}{\partial t} + \frac{\partial}{\partial x}(u_0 N) + \frac{\partial}{\partial y}(v_0 N) = -gh \frac{\partial \eta}{\partial y} - \frac{\tau_y}{\rho} \quad (7)$$

$$\frac{\partial h}{\partial t} + \frac{\partial M}{\partial x} + \frac{\partial N}{\partial y} = 0 \quad (8)$$

where

h	Height of water column within a mesh;
η	Elevation of water surface above sea level datum;
u_0, v_0	Velocity of a water column in X and Y directions, respectively (velocity distribution in Z direction is neglected, and assumed to be a constant);
M, N	Discharge of water per unit width in X and Y directions respectively ($M = u_0 h, N = v_0 h$);
g	Acceleration due to gravity.

Manning's basal resistance R(Manning) is expressed as below:

$$\text{X-component} : \frac{\tau_x}{\rho} = \frac{gn^2}{h^{7/3}} M \sqrt{M^2 + N^2}$$

$$\text{Y-component} : \frac{\tau_y}{\rho} = \frac{gn^2}{h^{7/3}} N \sqrt{M^2 + N^2}$$

ρ	Density of sea water;
n	Manning's roughness coefficient.

Visual Presentation of the Simulation Results by LS-RAPID and LS-Tsunami

Figure 2 shows the three steps of the series of landslide-induced tsunami simulation. The first step is landslide motion simulation by LS-RAPID. The second step is the tsunami simulation by LS-Tsunami using the calculated landslide motion data. The third step is visual presentation stage without calculation. The landslide and tsunami motions are visually

presented without calculation by a viewing code “LS-Motion” with different speed (time span of each image), color, balls/contours/three dimensional view/two dimensional view, photos, and video. The visual presentation of landslide hazard assessment and tsunami hazard assessment is important for risk management.

- Case A: Maximum depth = 100 m. Maximum length = 500 m, Maximum width = 300 m, Volume = $5.8 \times 10^6 \text{ m}^3$
- Case B: Maximum depth = 313 m. Maximum length = 1230 m, Maximum width = 1000 m, Volume = $170 \times 10^6 \text{ m}^3$.

4 Application of the Model to Two Hypothetical Simple Coastal Landslides

The new landslide-induced tsunami simulation was initially applied to two hypothetical landslides (A and B) on an imaginary slope.

The top of the slope was flat, the slope angle was 35° , and the bottom of the slope was a flat sea bed. The peak friction angle (ϕ_p) was 42° and the friction angle during motion (ϕ_m) was 40° . The heads of both landslides are at the top of the slope, and the toes of both landslide are at the water surface. The distance between the left end and the coast is 2000 m, and the distance from the coast to the bottom of the figure is 100,000 m in Figs. 3 and 4.

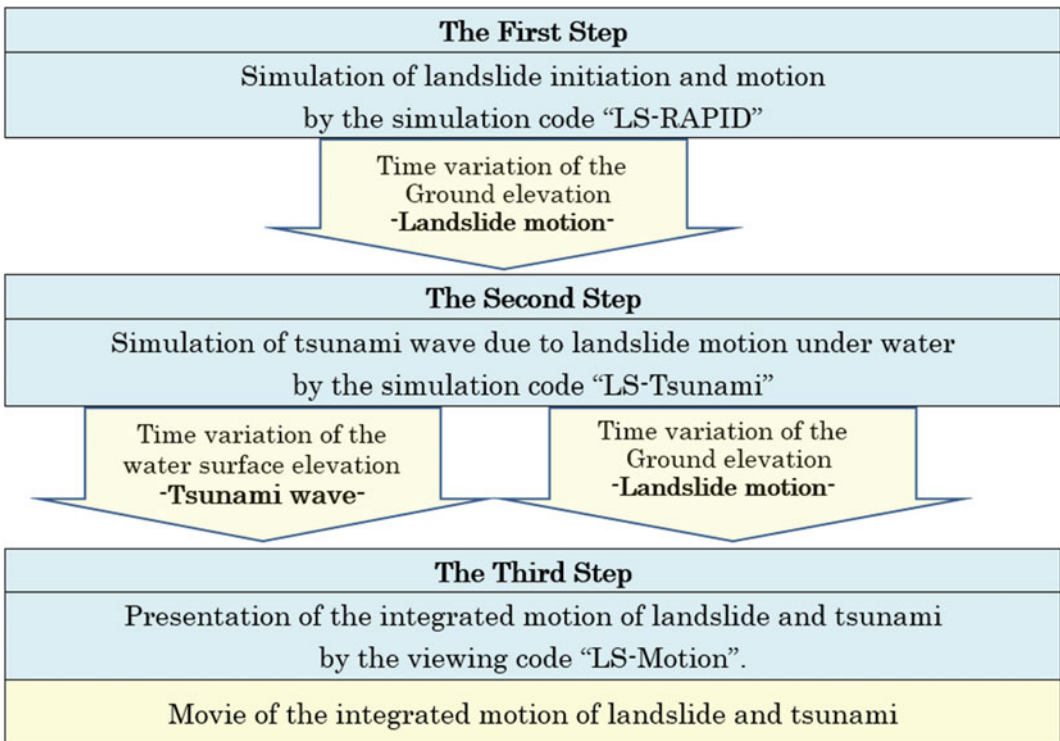


Fig. 2 Three steps of the landslide-induced-tsunami simulation

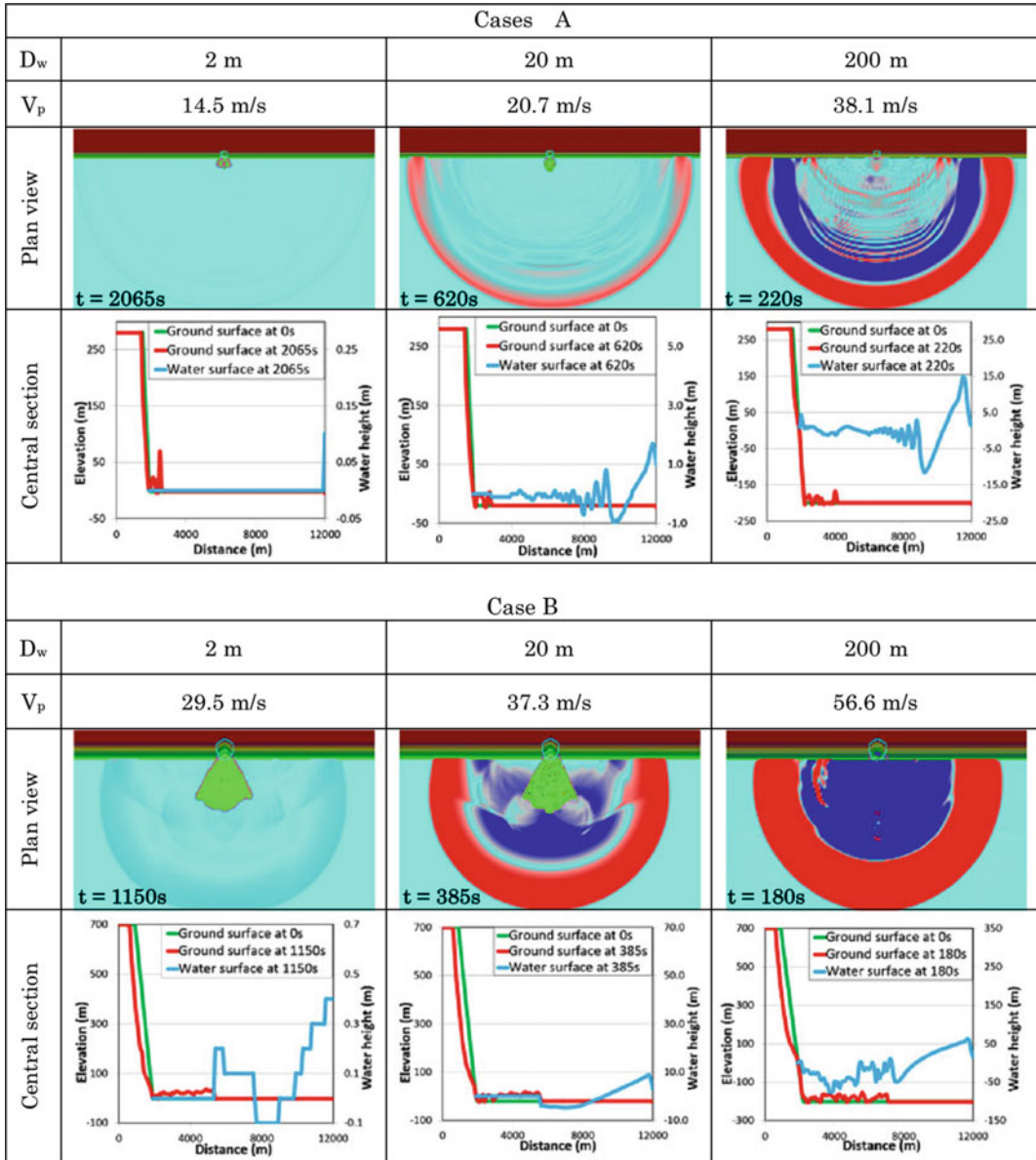


Fig. 3 Tsunami and landslide profiles when the tsunami front reached at 12,000 m

Definition of the maximum landslide velocity and the maximum tsunami height in Tables 1 and 2 are as follows.

- The *maximum landslide velocity* is the maximum velocity within the landslide mass when the front of the landslide mass reaches the flat sea/lake floor. Landslide velocity is one of indexes of triggering of tsunami as well as the landslide depth and the water depth.
- The *maximum tsunami height* is the maximum height in the tsunami profile (in Figs. 3

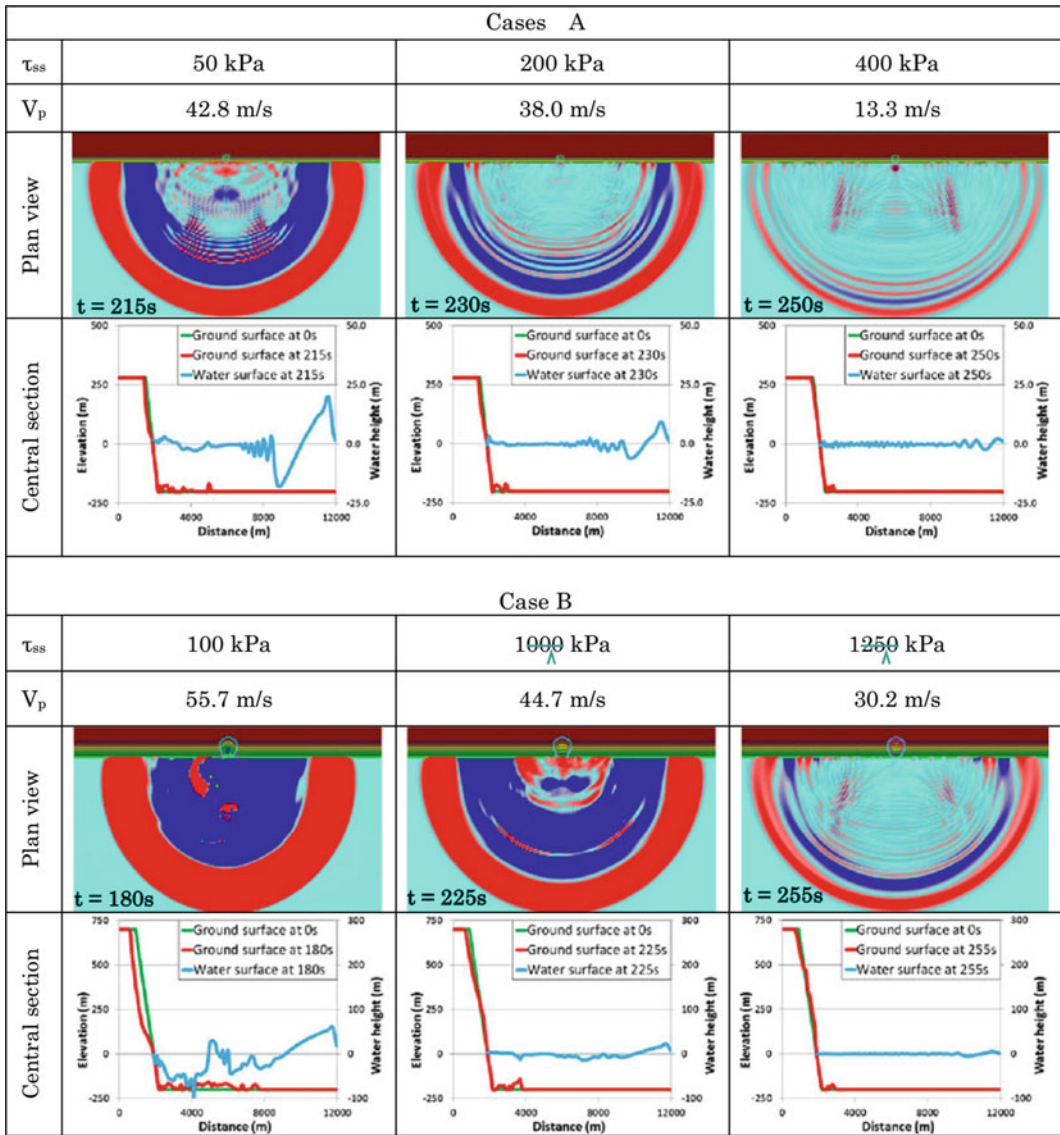


Fig. 4 Tsunami and landslide profiles when the tsunami front reached at 12,000 m

Table 1 Relation between water depth and tsunami behavior (steady state shear resistance = 80 kPa)

Landslide volume	Depth of water (m)	Maximum landslide velocity (m/s)	Tsunami traveling time (s) to 10 km from the coast	Maximum tsunami height (m) in Fig. 3
A: $5.8 \times 10^6 \text{ m}^3$	2	14.5	2,065	0.1
	20	20.7	620	1.7
	200	38.1	220	14.7
B: $170 \times 10^6 \text{ m}^3$	2	29.5	1,150	0.4
	20	37.3	385	8.7
	200	56.6	180	62.0

Table 2 Relation between the steady state shear resistance and tsunami behavior (depth of water is 200 m)

Landslide volume (m ³)	Steady state shear resistance (kPa)	Maximum landslide velocity (m/s)	Tsunami traveling time (s) to 10 km from the coast	Maximum tsunami height (m) in Fig. 4
A: 5.8 × 10 ⁶	50	42.8	215	20.0
	200	38.0	230	9.2
	400	13.3	250	2.2
B: 170 × 10 ⁶	100	55.7	180	62.0
	1000	44.7	225	23.4
	1250	30.2	255	5.9

and 4) when the front of tsunami reaches 10 km from the coast. It is an index of tsunami effect over a sea/lake.

The motion of tsunami is calculated at each 0.05 s, but the profiles in Figs. 3 and 4 and 2 D views in Fig. 8 are outputted and saved as the figures at each 5 s.

Figure 3 and Table 1 shows the relation between the water depth and the tsunami behavior at a constant steady state shear resistance (80 kPa), and different water depths (2, 20, 200 m).

The maximum tsunami heights are from 0.1 to 62.0 m. It increased with the depth of water and the landslide volume. As the depth of water increases, the maximum landslide velocity increases because the longer acceleration will increase landslide velocity on the longer steep slope below sea level. The larger volume of water in the deeper water depth is upheaved by the moving landslide mass and causes the greater tsunami height.

Figure 4 and Table 2 shows the relation between the steady state shear strength and the tsunami behavior at a constant water depth (200 m), and different steady state shear resistance. As the steady state shear resistance increases, the maximum velocity decreases, and also the maximum tsunami height decreases. The relationships between the maximum tsunami height and the tsunami traveling time is inversely proportional in Table 1. However, the effect of steady state shear resistance and the maximum landslide velocity on the tsunami traveling time is limited at the same water depth (Table 2).

5 Application of the Model to the Unzen-Mayuyama Landslide and Its Resulting Tsunami Wave

The 1792 Unzen-Mayuyama Landslide and Its Analysis

The series of landslide-induced tsunami simulation LS-RAPID + LS-Tsunami + LS-Motion was applied to the 1792 Unzen-Mayuyama landslide-and-tsunami disaster. Figure 5 presents a Google view of the landslide. The displaced landslide mass created many islands in the Ariake Sea. Most of them disappeared by sea erosion after the event. But some landslide mounds still exist as islands. Figure 6 presents the section of this landslide (Sassa et al. 2014a, b, modified from the Unzen Restoration Office of the Ministry of Land, Infrastructure, and Transport (MLIT) of Japan, 2002 and 2003). The Unzen-Mayuyama mountain consists of volcanic lava rock and unconsolidated eruption products (sand and debris). Two samples (S1 and S2) were taken from the site for testing to obtain the landslide dynamic parameters by the undrained dynamic-loading ring-shear apparatus (Sassa et al. 2014a, b). The sliding surface of the landslide should be formed within a sandy layer rather than in a layer consisting of strong intact lava rocks and boulders. Hence, sample S1 was taken from a sandy layer exposed along a torrent gully in the source area of the landslide. The original soil layer (a black dotted soil layer in

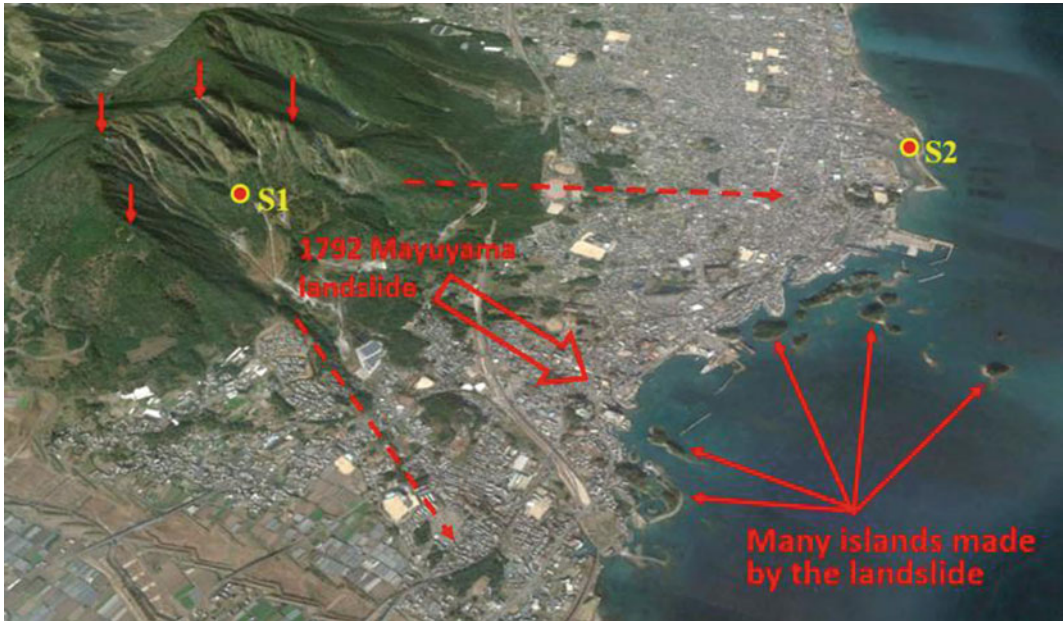


Fig. 5 1792 Unzen-Mayuyama landslide. The overview of the landslide. The headscarp is indicated by *vertical red arrows*, the direction of the landslide motion is shown by a *thick red arrow* in the center and *two dotted lines* in the sides

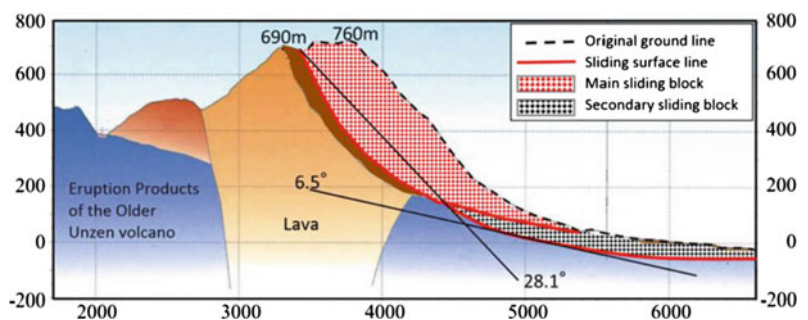
Fig. 6) was displaced or covered by the moved landslide mass and the original soil layer could not be found at the site. Hence, a sample S2 representing this soil layer was taken from the coastal area outside of the landslide moving area.

The necessary landslide dynamics parameters were measured and estimated by a series of undrained ring shear tests; drained speed-control test, undrained monotonic shear-stress loading test, pore pressure control test to simulate landslide initiation by pore pressure increasing, undrained cyclic-loading test, and undrained pore pressure and seismic-loading test simulating the

earthquake-induced landslide in the Mayuyama landslide (Sassa et al. 2014a, b).

The landslide is known to have been triggered by a nearby earthquake (of estimated magnitude, $M = 6.4 \pm 0.2$, Usami 1996). The amount of damage to houses caused by the earthquake suggests that the seismic acceleration was 400 cm/s^2 or greater (Unzen Restoration Office 2002, 2003). There is no seismic wave record from this earthquake which predates recording seismometers. So we used a recent seismic record (MYG004 that of the 2008 Iwate Miyagi-earthquake, $M = 7.2$, which triggered the 67 million m^3 Aratozawa landslide, maximum

Fig. 6 Section of the 1792 Unzen-Mayuyama landslide and its interpretation



acceleration was 739 cm/s^2 (Sassa et al. 2014a, b) for the seismic shear stress loading in the undrained ring shear test. The test result showed that the necessary maximum acceleration to initiate this landslide was 216 cm/s^2 . It means that the smaller earthquake can produce this landslide. Then, 0.7 times and 0.5 times of the acceleration of MYG004 (507 and 370 cm/s^2) were input to LS-RAPID. Both cases gave the very similar result of landslide motion. We used 0.5 times of MYG004 (Maximum acceleration of 370 cm/s^2) was given as the triggering factor to LS-RAPID. The landslide dynamics parameters used in this simulation are shown in Table 3.

Simulation of the Unzen-Mayuyama Landslide by LS-RAPID

The simulation area for the landslide-induced tsunami including the Ariake Sea and Kumamoto Prefecture on the opposite bank is $59 \text{ km} \times 37.4 \text{ km}$. It is much wider than the simulation area for the Mayuyama landslide ($12 \text{ km} \times 8 \text{ km}$). Due to the computer capacity and the time for one simulation, the mesh size was increased from 50 m (used in the previous study of 2014, Sassa et al. 2014a, b) to 100 m in this landslide-induced tsunami study. The results from the landslide simulation are shown in Fig. 7.

LS-RAPID has two presentation modes showing the moving landslide mass. One mode is color balls with different sizes and different color intensities for the landslide depth which was used for the Leyte landslide simulation in Fig. 12 of Sassa et al. (2010). This makes it easier to visualize the landslide motion. However, it does not show the real ground surface of the landslide during motion. Another mode is either a three-dimensional or a two-dimensional view of the moving landslide. The three-dimensional view is suitable to visually show the motion. However, the two dimensional-view is good for the precise location as a map. 4 Figures of Fig. 7 show a two-dimensional view of the landslide motion from the initiation to the termination. The initial landslide mass before

motion is delineated by a blue line and the moving landslide mass is delineated by a red line. The figure shows that the landslide mass moved into the Ariake Sea, and tops of moving landslide masses appeared above the sea and stopped its motion partly filling the Shimabara port. After the 1792 Unzen-Mayuyama landslide event, coastal erosion changed the topography of this port because most of displaced landslide masses were weak to coastal erosion. But some strong parts are still left as islands in the sea as seen in Fig. 5.

Simulation of the Landslide-Induced Tsunami by LS-Tsunami

The yellow color line is the coastal line before the landslides. The red line is the border of displaced landslide mass. The left-top figure ($t = 0 \text{ s}$) presents the location of the initial landslide mass, the right-top figure ($t = 35 \text{ s}$) presents the instant when the landslide moving mass reached the coast. The left-bottom figure ($t = 100 \text{ s}$) shows the moving landslide mass in the Ariake Sea. Parts of moving landslide blocks (gray color parts) are found above the sea. The right-bottom figure ($t = 226 \text{ s}$) presents the state when the landslide motion was terminated.

The landslide motion was firstly calculated by LS-RAPID as Fig. 7. The data set of calculated landslide motion at each 0.1 s was saved, and used as input to LS-Tsunami as the tsunami trigger. Additional parameters input in the LS-Tsunami is the unit weight of sea water and the Manning's roughness coefficient for basal resistance in the sea. The Manning's roughness coefficient is not testing value, but an empirical value used for analysis of water movement such as tsunamis and floods. Tsunami motion generated by the landslide motion was calculated by LS-Tsunami. The result of simulated tsunami height at each mesh and at each 0.05 s was saved. These data sets were then used as input to LS-Motion. The tsunami simulation is shown in whatever preferred mode, color, and speed by LS-Motion. Figure 8 is an example from

Table 3 Parameters used in computer simulation of Unzen-Mayuyama landslide-and-tsunami disaster

Parameters used in simulation	Value	Source
<i>Parameters of soils in the source area (deeper area)</i>		
Steady state shear resistance (τ_{ss})	120 kPa	Test data
Lateral pressure ratio ($k = \sigma_h/\sigma_v$)	0.7–0.8	Estimation (see text)
Friction angle at peak (ϕ_p)	42.0°	Test data
Cohesion at peak (c)	10 kPa	Assuming small
Friction angle during motion (ϕ_m)	40.0°	Test data
Shear displacement at the start of strength reduction (D_L)	6 mm	Test data
Shear displacement at the start of steady state (D_U)	90 mm	Test data
Pore pressure generation rate (B_{ss})	0.7–0.9	estimated
Total unit weight of the mass (γ_t)	19.5 kN/m ³	From the test
Unit weight of sea water (γ_w)	10.1 kN/m ³	Average sea water density (1.026 kg/m ³)
<i>Parameters of soils in the moving area (shallower area)</i>		
Steady state shear resistance (τ_{ss})	30–80 kPa	Test data
Lateral pressure ratio ($k = \sigma_h/\sigma_v$)	0.8–0.9	Estimated
Friction angle at peak (ϕ_p)	40.0°	Test data
Cohesion at peak (c)	10 kPa	Assuming small
Friction angle during motion (ϕ_m)	40.0°	Test data
Shear displacement at the start of strength reduction (D_L)	6 mm	Test data
Shear displacement at the end of strength reduction (D_U)	90 mm	Test data
Pore pressure generation rate (B_{ss})	0.7–0.9	Estimated
Total unit weight of the mass (γ_t)	19.5 kN/m ³	From the test
<i>Triggering factor</i>		
Excess pore pressure ratio in the fractured zone (r_u)	0.21	Assumption
0.5 times of the 2008 Iwate-Miyagi earthquake	Max: 370 cm/s ²	Wave form of the Ground motion record at MYG004
<i>Parameters of the function for non-frictional energy consumption</i>		
Coefficient for non-frictional energy consumption	1.0	See Sassa et al. 2010
Threshold value of velocity	100 m/s	A few times greater than maximum reported speed
Threshold value of soil height	400 m	Maximum depth of the initial source area
<i>Other factors</i>		
Steady state shear resistance under sea	10 kPa	Data (Sassa et al. 2004)
Unit weight of sea water	10.1 kN/m ³	Average sea water density
Manning's roughness coefficient	0.025	Under water and vacant lots (MLIT Guideline 2012)

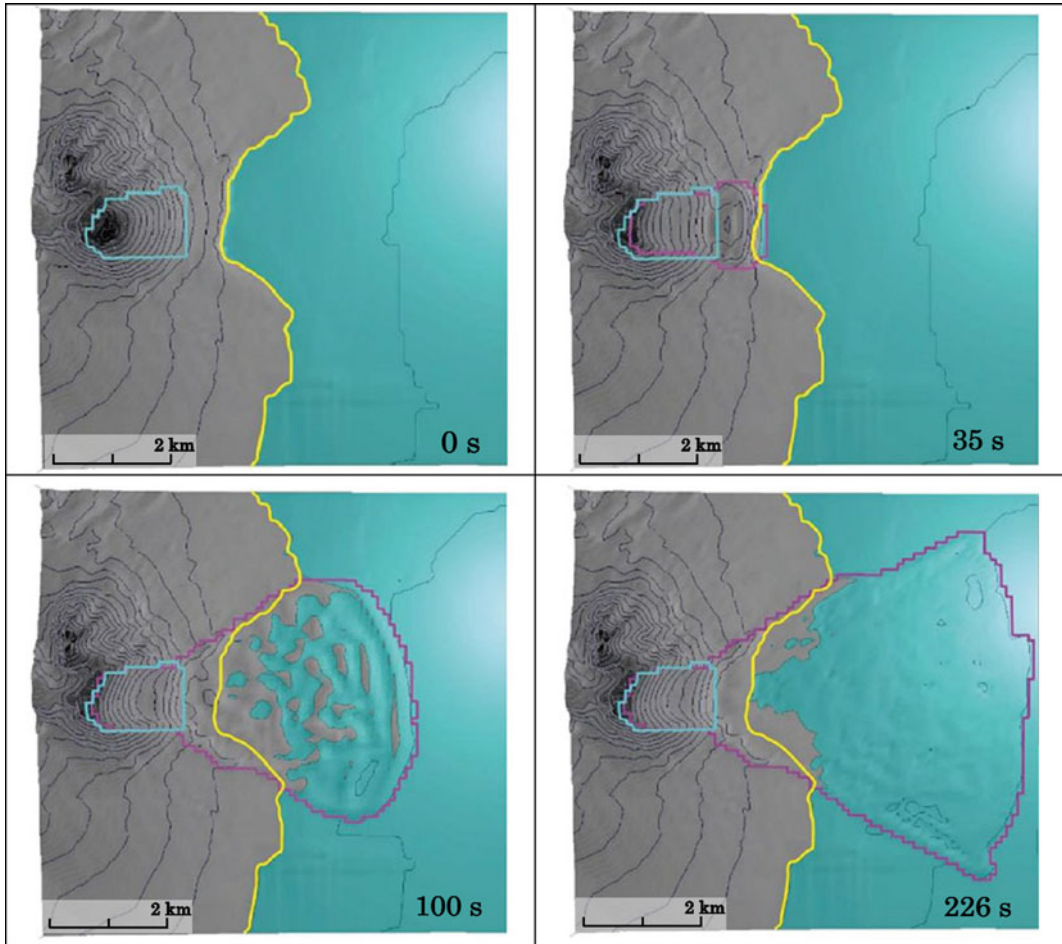


Fig. 7 Landslide motion simulated by the landslide simulation code “LS-RAPID”

LS-Motion. The explanation/interpretation of the behavior of landslide and tsunami at each figure of Fig. 8 is directly written in the caption.

The tsunami disaster investigated by the Unzen Restoration office (2002, 2003) is shown in Fig. 9. The residents in the community erected the Tsunami-Dome-Ishi (tsunami stopping stones) at the highest points where the tsunami reached. Tsunami-Dome-Ishi are found in Kyodomari, in Umedo and in Ohtao along the coast of Kumamoto Prefecture, which were carefully investigated by Tsuji and Hino (1993). People in the Shimabara Peninsula built stone pillars in memory of the tsunami disasters. Tsuji and Murakami (1997) investigated Tsunami heights in the Shimabara Peninsula. Figure 9 was made

using those investigation, the historical data as well as stone pillars.

The original file of Fig. 9 is a Japanese printed figure. It can not be changed. English explanation is written in the figure caption 8 by adding A-I within Fig. 9. *Shimabara-Taihen, Higo-Meiwaku*. in A is a lesson from this historically largest landslide and volcanic disaster. We should not neglect disasters in the opposite bank. Adverse effects may reach the opposite bank.

Five sites (3 sites from the Kumamoto coast and 2 sites from Shimabara coast) with clearer evidences were selected to compare the results simulated by the LS-Tsunami based on LS-RAPID to the tsunami heights by historical records in both coasts. The maximum tsunami

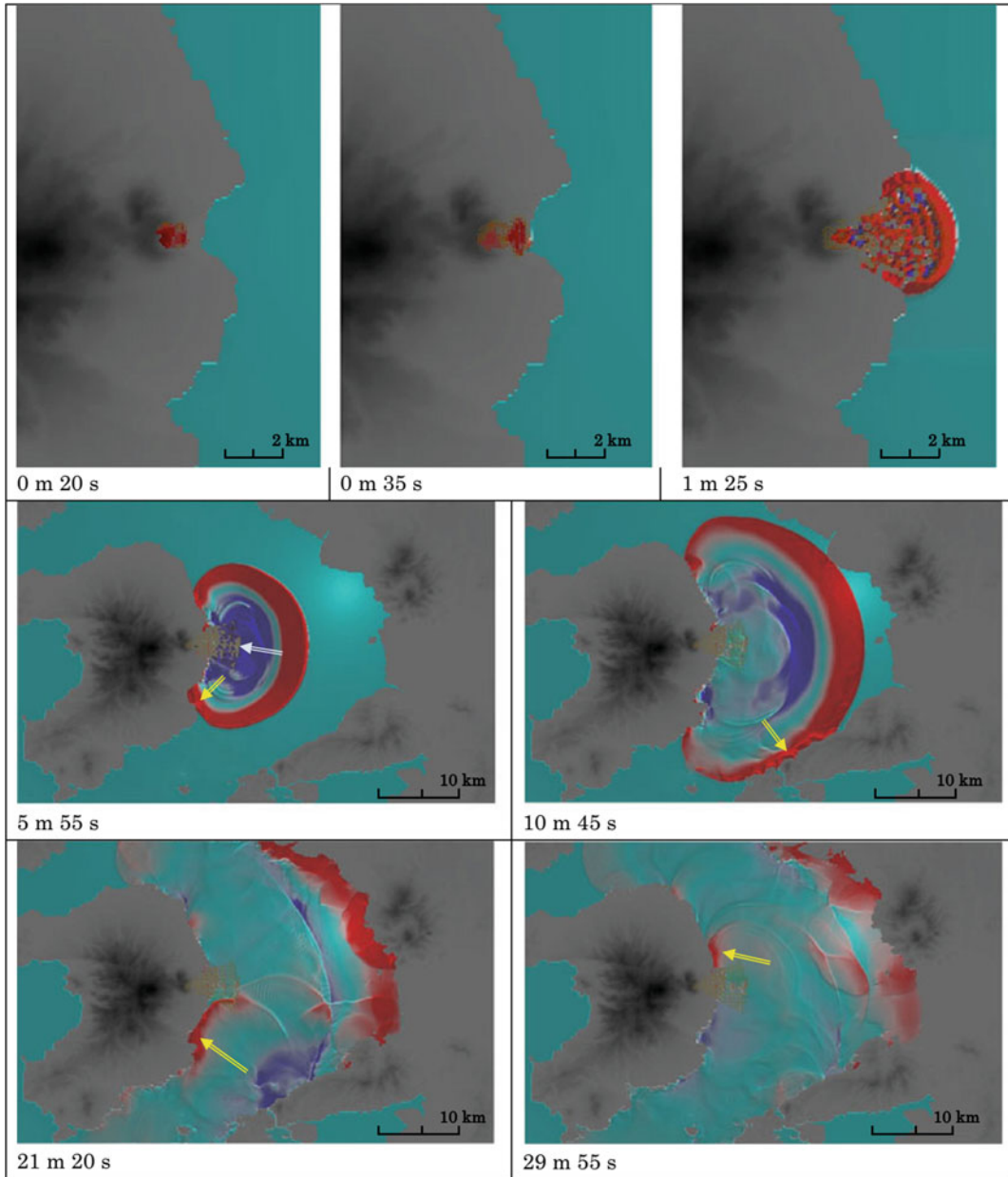


Fig. 8 Simulation result of Landslide-induced-tsunami wave using the simulation code “LS-Tsunami” and “LS-Motion”. The *first figure on the top* shows when the initial landslide started to move at 0 min 20 s. The *second figure on the top* at 35 s shows the landslide mass reached the coastal line and triggering the tsunami wave. The *third figure on the top* at 1 min 25 s shows the landslide mass entering into the sea and triggering the tsunami wave. The *left figure* (5 min 55 s) in the center shows the expanding tsunami wave into the Ariake Sea, and the top parts of moving landslide blocks (dark brown color dots) are seen above sea level as shown by a white color arrow. The yellow color arrow shows the attack of tsunami wave to Futsu town. The

right figure in the center presents when the tsunami wave reached Kumamoto Prefecture on the opposite bank. The *left figure* (21 min 20 s) on the bottom shows that the tsunami wave was returned from the opposite bank to attack the southern part of Shimabara peninsula (around Futsu town) again as shown in the yellow arrow. Around 3500 persons were killed in the southern part of Shimabara peninsula by the Tsunami (Fig. 9). The *right figure on the bottom* at 29 min 55 s shows another returned wave attacking the northern side of Mayuyama landslide area. In this figure, the bright red color presents the wave more than 5 m above sea level and the dark blue color presents the wave less than 5 m below sea level



Fig. 9 Records of disaster by the Unzen landslide-and-tsunami disaster (by Unzen Restoration Office 2003)

heights at each 0.05 s for each mesh were plotted on the map and the contour map was made to visualize the tsunami wave (Fig. 10). Locations of these five sites are shown in this figure. The simulated tsunami wave reached more than 5 km inland on the Kumamoto coast.

Comparison was conducted between:

1. Tsunami heights estimated from the simulation (LS-RAPID and LS-Tsunami) based on the values of landslide dynamics parameters measured and estimated by the undrained ring shear testing on the samples taken from the site.
2. Tsunami heights reported by the Unzen Restoration office (2002, 2003) based on the

records including Tsuji and Hino (1993) and Tsuji and Murakami (1997) in the Shimabara and Kumamoto areas. Tsunami heights in the sea were not recorded. But the landslide depth under the sea was investigated and reported by the office.

Manning’s roughness coefficient

The simulated tsunami heights are affected by the value of Manning’s roughness coefficient. The coefficient was reported to be between 0.010 and 0.060 m^{1/3} s as empirical values in the cases of water channels with different materials (Linsley and Franzini 1979). The coefficient used for Tsunami simulation were reported between 0.01 and 0.08 m^{1/3} s by many reports and guidelines

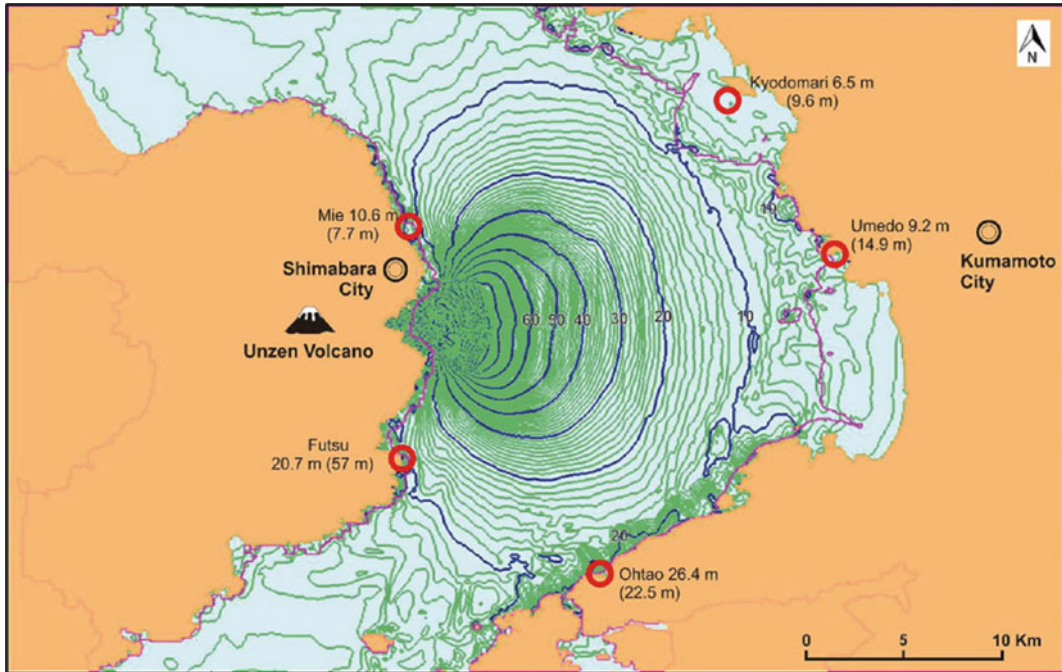


Fig. 10 Contour of the maximum tsunami height at each mesh with the tsunami height records in the Kumamoto side coast and in the Shimabara side coast. The coastline is shown in red where the tsunami wave moved up to the land

such as MLIT 2012, Fraser et al. 2014, Imamura 2009, Tinti and Tonini 2013. $0.03\text{--}0.08\text{ m}^{1/3}\text{ s}$ are used for forests and buildings areas. The most commonly used value of Manning's coefficient for tsunami simulation is $0.025\text{ m}^{1/3}\text{ s}$ (MLIT 2012; Tinti and Tonini 2013; Imamura 2009). The purpose of this research is not examination of the value of Manning's roughness coefficient, but the examination of the reliability of the new landslide-induced tsunami simulation. Then, we used the most commonly used value of $0.025\text{ m}^{1/3}\text{ s}$ for Figs. 8 and 10 of this paper.

Total number of death is 15,153 persons. The size of circles is proportional to the number of human fatalities in the area. The legend for the number of deaths is show in the right-top corner. A: Disasters around Ariake sea and monuments by the *Shimabara-Taihen*, *Higo-Meiwaku*. "Catastrophe" in Shimabara area and "Annoyance" or "adversely affected" in Higo (Kumamoto) region. B: The numbers of deaths are shown in the circles (the largest is 500 persons) C: The greatest deaths are Shimabara town

around the castle (5251 persons). D: The second largest deaths are the southern part of Shimabara Peninsula (around 3500 persons) E, F, G: Tsunami-Dome-Ishi (A stone showing the tsunami reaching point) was set to record the tsunami by the community in Kyodomari (E), Umedo (F) and Otao (G) of the Higo (Kumamoto) Han area. The tsunami-Dome-Ishi in Kyodomari was moved for the construction of a road, but its former location is marked on the road retaining wall (by the regional education committee). The Tsunami-Dome-Ishi is limited in Higo (Kumamoto) Han area. These tsunami records are reliable. H, I: Stone pillars for memorial service for deaths by Tsunami in Futsu (H) and Mie (I) in Shimabara Han area.

Manning's basal resistance is caused by the roughness of the ground surface during relative movement of water on the ground. When water depth is greater, the effect of basal resistance for the movement of tsunami will be decreased and the value will be smaller. The deposits in the deeper sea is usually finer, then the roughness is

decreased. Fraser et al (2014) used $0.013 \text{ m}^{1/3} \text{ s}$ for ocean and rivers. Ariake Sea which is the major part of Tsunami propagation in this area is 10–50 m deep. It is deeper than pond, river and shallow sea near coast. Therefore, we examined the case of 0.02 and $0.015 \text{ m}^{1/3} \text{ s}$ in addition to $0.025 \text{ m}^{1/3} \text{ s}$ in Table 4.

Comparison of Tsunami Heights Between Historical Records and Simulation Results

Table 4 presented the reported and simulated tsunami heights at 5 sites along the Kumamoto and the Shimabara coasts. Differences between the computer simulation and the historical records for the 5 specific points are less than 5.7 m for Manning's coefficient $0.025 \text{ m}^{1/3} \text{ s}$, 4.6 m for Manning's coefficient $0.020 \text{ m}^{1/3} \text{ s}$, and 5.2 m for Manning's coefficient $0.015 \text{ m}^{1/3} \text{ s}$ except the case at Futsu.

Futsu is a special case where the first direct tsunami wave from the source of tsunami hit the cliff of the Futsu terrace, and probably amplified due to the gulf-shaped coast line. The tsunami wave flowed up to the Terrace (Tsuji and Murakami 1997). The Tsunami wave attacking Futsu is seen at 5 m 55 s in Fig. 8 and the return wave also attacked Futsu from the different direction at 21 m 20 s in Fig. 8. Many people were killed in this area. The simulation of LS-Tsunami used 100 m mesh data. It can not include the effect of local amplification of tsunami height due to the sharp topography in this part of the coast.

LS-Tsunami uses the average elevation for each 100 m mesh. The elevation of Tsunami-Dome-Ishi on the slope is not always

close to the average height of calculated mesh. In the case of 15–20° slope, 25 m (1/4 of one mesh) difference in horizontal distance cause 6.7–9.1 m elevation difference. The maximum 5.7 m difference in Table 4 is within the elevation difference on the slope. Considering these conditions, the estimated area of tsunami and the tsunami heights along the coast by LS-Tsunami match with the historical record (Fig. 10 and Table 4). It can be understood that the result of this trial test on the Unzen-Mayuyama landslide-and-tsunami disaster presented a reasonable extent of reliability and a meaningful extent of precision within the variation of Manning's coefficient and the resolution of ground elevation. Carefully examining the value difference in different Manning's coefficient, the effect of the coefficient is greater in the long travel distance of tsunami and gives closer tsunami heights in Kyodomari and Umedo.

Comparison of the Maximum Heights of the Landslide and the Maximum Heights of Tsunami Along the Central Section

The upper figure of Fig. 11 presents the maximum landslide moving height and the maximum tsunami height calculated by LS-RAPID and LS-Tsunami at each time step (0.1 s for landslide, and 0.05 s for tsunami wave) at each mesh along the central line of landslide. The ground surface before the landslide and the ground surface after the deposition of the landslide were investigated by Inoue 1999 and MLIT 2002 and 2003. The lower figure of Fig. 11 presents the central section of ground surface before and after the landslide. The landslide travel distance

Table 4 Comparison of Tsunami heights between the simulation result and the historical record

Location		Tsunami heights from tsunami-Dome-Ishi and memorial stone pillars (m)	Tsunami heights by LS-tsunami Manning's coefficient = $0.025 \text{ m}^{1/3} \text{ s}$ (m)	Tsunami heights by LS-tsunami Manning's coefficient = $0.020 \text{ m}^{1/3} \text{ s}$ (m)	Tsunami heights by LS-tsunami Manning's coefficient = $0.015 \text{ m}^{1/3} \text{ s}$ (m)
Kumamoto coast	Kyodomari	9.6	6.5	7.7	9.7
	Umedo	14.9	9.2	11.2	13.2
	Ohtao	22.5	26.4	27.1	27.7
Shimabara coast	Futsu	57	20.7	21.0	21.3
	Mie	7.7	10.6	10.9	11.0

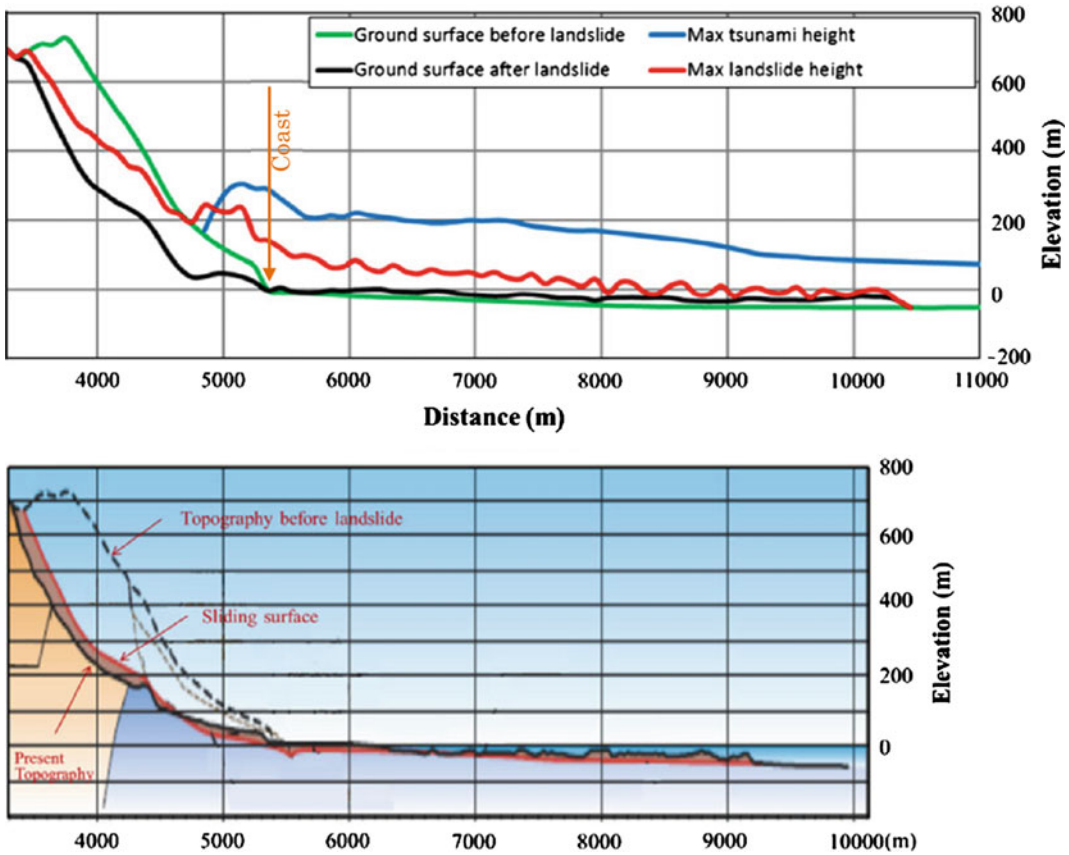


Fig. 11 The simulated maximum heights of tsunami wave and the landslide mass (*top*) and the central section of landslide reported by MLIT (*bottom*)

estimated by LS-RAPID is a little longer than the real one. However, the horizontal distance from the headscarp to the landslide toe is around 10,000 m in both cases. The highest landslide mass above the original ground surface near the coast is 127 m at the time resolution of 0.1 s. The highest tsunami height near the coast is 70 m higher than the surface of the moving landslide mass at the time resolution of 0.05 s.

The landslide dynamics research group and the tsunami research group cooperated to develop the landslide-induced tsunami model. Based on the joint research, the tsunami research group earlier developed a soil and water double layer model and applied it to the 1792 Unzen-Mayuyama landslide-induced tsunami (Yanagisawa et al. 2014). The model calculates movement of two layers: a water layer and a soil

layer, with simultaneous interaction of the two layers. While the proposed model fully separated the motion of landslide and the motion of tsunami. The landslide motion was given to the tsunami simulation as the trigger only. The tsunami simulation model is a well established and widely used one (IOC 1997). This study could not have been completed without the close cooperation between hydraulics researchers and landslide researchers.

6 Conclusion

Hazard assessment technology for landslide-induced tsunami is one of the frontiers in Landslide Science. A tsunami wave is induced by the landslide mass entering into and moving

under the water. The reliable estimation of landslide motion is the most important as the trigger of the landslide-induced tsunami hazard. The integrated model simulating the initiation and the motion of landslide (LS-RAPID) and the measurement of the landslide dynamics parameters by the undrained dynamic-loading ring-shear apparatus enabled estimation of the landslide motion as the trigger of a tsunami wave. The concept of tsunami simulation (LS-Tsunami) is simple: a water mass is elevated by a landslide mass moving on the sea floor. The increased water height causes a tsunami wave. Possible shear resistance between the landslide mass and water due to viscosity is neglected because it is much smaller than the shear resistance mobilized along the shear surface within soils. The tsunami simulation model is a well established model (IOC 1997). The parameters used related to water were only the unit weight of sea water and the Manning's roughness coefficient without other uncertain parameters. This new landslide-induced tsunami model could provide a simulation result well matching the tsunami heights in the Unzen Mayuyama landslide-and-tsunami disaster. This result presented an evidence of reliability and precision of this new landslide-induced tsunami model in this well documented and historically largest landslide-induced tsunami in Japan. Further application to other cases of landslide-induced tsunami can define the reliability and precision of this new model from different aspects.

References

- Abe I, Goto K, Imamura F, Shimizu K (2008) Numerical simulation of the tsunami generated by the 2007 Noto Hanto Earthquake and implications for unusual tidal surges observed in Toyama Bay. *Earth Planets Space* 60:133–138
- Baba T, Matsumoto H, Kashiwase K, Hyakudome T, Kaneda Y, Sano M (2012) Microbathymetric evidence for the effect of submarine mass movement on tsunami generation during the 2009 Suruga bay earthquake, Japan. In: Yamada et al (eds) *Submarine mass movements and their consequences*. Advances in natural and technological hazards research 31. Springer, Berlin, pp 485–494
- Fraser SA, Power WL, Wang X, Wallace LM, Mueller C, Johnston DM (2014) Tsunami inundation in Napier, New Zealand, due to local earthquake sources. *Nat Hazard* 70:415–445
- Imamura F (2009) Tsunami modeling: calculating inundation and hazard maps. In: Bernard EN, Robinson AR (eds) *THE SEA tsunamis*. Harvard University Press, London, pp 321–332
- Inoue K (1999) Shimabara-Shigatsusaku Earthquake and topographic changes by Shimabara catastrophe. *J Jpn Soc Eros Control Eng* 52(4):45–54 (in Japanese)
- Intergovernmental Oceanographic Commission (IOC) (1997) Numerical method of tsunami simulation with the leap-frog scheme. IUGG/IOC Time Project IOC Manuals and Guides, No. 3, UNESCO
- Linsley RK, Franzini JB (1979) *Water resource engineering*, 3rd edn. McGraw-Hill, New York
- Ministry of Land, Infrastructure, Transport and Tourism (MLIT), Water and Disaster Management Bureau, Coastal management office (2012) *Guideline for the assessment for Tsunami inundation area*. Ver.1.00, http://www.mlit.go.jp/river/shishin_guideline/bousai/saigai/tsunami/shinsui_settei_ver100.pdf
- Sassa K, Fukuoka H, Wang G, Ishikawa N (2004) Undrained dynamic-loading ring-shear apparatus and its application to landslide dynamics. *Landslides* 1(1):7–19
- Sassa K, Nagai O, Solidum R, Yamazaki Y, Ohta H (2010) An integrated model simulating the initiation and motion of earthquake and rain induced rapid landslides and its application to the 2006 Leyte landslide. *Landslides* 7(3):219–236
- Sassa K, He B, Miyagi T, Strasser M, Konagai K, Ostric M, Setiawan H, Takara K, Nagai O, Yamashiki Y, Tutumi S (2012) A hypothesis of the Senoumi submarine megaslide in Suruga Bay in Japan-based on the undrained dynamic-loading ring shear tests and computer simulation. *Landslides* 9(4):439–455
- Sassa K, Dang K, He B, Takara K, Inoue K, Nagai O (2014a) A new high-stress undrained ring-shear apparatus and its application to the 1792 Unzen-Mayuyama megaslide in Japan. *Landslides* 11(5):827–842
- Sassa K, Bin H, Dang K, Nagai O, Takara K (2014b) Plenary: progress in landslide dynamics. *Landslide Sci Saf Geoenviron* 1:37–67
- Satake K (2001) Tsunami modeling from submarine landslides. In: *Proceedings of the international tsunami symposium*, pp 665–674
- Tinti S, Tonini R (2013) The UBO-TSUFSD tsunami inundation model: validation and application to a tsunami case study focused on the city of Catania, Italy. *Nat Hazards Earth Syst Sci* 13:1795–1816
- Tsuji Y, Hino T (1993) Damage and Inundation height of the 1792 Shimabara landslide tsunami along the coast

- of Kumamoto Prefecture. Bull Earthq Res Inst Univ Tokyo 68:91–176 (in Japanese)
- Tsuji Y, Murakami Y (1997): Inundation height of the 1792 Mayuyama landslide tsunami in the Shimabara Peninsula side. In: Historical earthquake, No. 13, Soc. of historical earthquake studies, pp 135–197
- Unzen Restoration Office of the Ministry of Land, Infrastructure and Transport of Japan (2002) The Catastrophe in Shimabara—1791–92 eruption of Unzen–Fugendake and the sector collapse of Mayu-Yama. An English leaflet
- Unzen Restoration Office of the Ministry of Land, Infrastructure and Transport of Japan (2003) The Catastrophe in Shimabara—1791–92 eruption of Unzen–Fugendake and the sector collapse of Mayu-Yama. A Japanese leaflet
- Usami T (1996) Materials for comprehensive list of destructive earthquakes in Japan. University of Tokyo Press, Tokyo (in Japanese)
- Yanagisawa H, Aoki A, Sassa K, Inoue K (2014) Numerical simulation of 1792 Ariake-Kai Tsunami using Landslide-Tsunami model. J Jpn Soc Civil Eng Ser. B2 (Coast Eng) 70(2):151–155 (in Japanese)